THE EUROPEAN
PHYSICAL JOURNAL D

The morphological and compositional changes of bimetallic Ti/Al thin film induced by ultra-short laser pulses

B. Gaković[1,a], P. A. Danilov[3], S. I. Kudryashov[3], D. Milovanović[2], A. Radulović[2], P. Panjan[4], and A. A. Ionin[3]

[1] Vinča Institute of Nuclear Sciences, 11000 Belgrade, Serbia
[2] Institute of General and Physical Chemistry, Belgrade 11000, Serbia
[3] Lebedev Physical Institute, Russian Academy of Sciences, Moscow 119991, Russia
[4] Jožef Stefan Institute, Ljubljana 1000, Slovenia

Abstract. Results regarding morphological and compositional changes of bimetallic thin film (BMTF), composed of aluminium (Al) and titanium (Ti) nano-layers, by single fs laser pulses, are presented. Laser irradiation was conducted in the air with focused, linearly polarized laser pulses, the duration being 300 fs, wavelength 515 nm, and pulse energy up to 1.2 µJ. Effects of the variations of the pulse energy on the changes were studied. In the experiment, single pulse energy values from 0.03 to 0.08 µJ caused ablation–photomechanical spallation of the upper part of BMTF layer from the Si substrate, without ablation of the whole film. Irradiation at higher pulse energies gradually removed the whole BMTF and even a part of the Si substrate. We explained the influence of different electron–phonon dynamics, in the case of multilayered thin films composed of Al and Ti, on BMTF ablation. Damage/ablation threshold, which is minimal pulse energy/fluence sufficient for starting ablation, was calculated.

1 Introduction

Thin films are important for many applications, ranges from decoration and protection of materials, through technological usage to environmental and medical purposes. Multilayer structures, composed of two or more materials (nanometre thicknesses) broaden and improve the thin film usage [1–4]. As a result, multilayer thin films can be found in contemporary technics, nanotechnology, optical devices, photovoltaic and gas sensors, microelectronics, plasmonics, soft X-ray and neutron devices, such as super mirrors, polarizers, monochromators, etc. Among them, Al and Ti thin films bilayer are suitable for many of the mentioned applications [3].

The method that supports exceptionally controlled non-contact morphological and composition modifications of materials is laser processing. The effect of laser action on materials depends on several factors, such as laser parameters (wavelength, pulse duration, pulse energy, fluence, etc.), material characteristics (physicochemical properties, surface state, reflectivity, etc.), and an environment during radiation [5]. Up to now, the individual thin films and their combinations have been studied regarding irradiation with short nanosecond (ns) [6,7] and ultra-short picosecond and femtosecond (ps and fs) laser pulses [8–14]. In the case of fs pulses, this method allows extremely precise modifi-

cations, on the micrometre and even on the nanometre scale. Accurate results are obtained with fs pulses because of suppressing the formation of a heat-affected zone, which is vital for ultrahigh precision fabrication [15]. For precise surface modification of multi-layer thin films, the thermodynamic and mechanical properties of adjacent layers, interlayer adhesion, and boundary thermal resistance significantly affect the results of micro-/nano-processing, such as the possibility of selective removal of the required layers [16,17].

Fs laser irradiation of metals is known to proceed via multiple steps as (1) absorption of photon energy including photoexcitation of electrons, (2) energy transfer from electrons to the lattice, (3) melting and thermal expansion, (4) damage of the surface without or with ablation, and in some cases photomechanical spallation, and (5) thermal relaxation. The cases (1) and (2) highly depend on the specific metal zone structure and are the most important at low laser beam fluence, i.e. the ratio between laser pulse energy and laser beam sectional area. The knowledge of these processes is crucial for understanding the experimental, observations for predicting the damage and/or ablation thresholds of a material that is significant for the development of laser nanotechnology in general

Further, following the steps (3) to (5), irradiation at higher pulse energy/fluence is important for precise laser nanofabrication of metals either in the bulk

[a] e-mail: biljagak@vin.bg.ac.rs (corresponding author)

or in the thin film forms. It was shown that there is a "window" of the laser fluences at which specific ablation–photomechanical spallation is registered. Spallation brings about the irradiated region of the surface having a characteristic crater with a flat centre and a sharp edge. Theoretical explanations and examples of photomechanical spallation can be found elsewhere [18–22]. In the conducted experiment with the single fs laser pulses and BMTF we estimated damage threshold laser fluence and found the "window" of the laser fluences that caused selective ablation/spallation of the first nano-layer and a part of the bottom one. Morphological and compositional changes of the irradiated spots/craters, produced by single pulses for all used fluences, were studied.

2 Experiment

The sample BMTF that was used in the experiment is composed of two layers, titanium and aluminium. The first layer deposited on the silicon (Si) substrate was Ti, and the second, the top layer, was Al. The deposition was performed in a triode sputtering system Sputron (Balzers Oerlikon). The BMTF deposition was started and stopped by opening or closing the moveable shutters between the substrate holder and sputter source (target). High-purity targets were used as the sputtering source. With average d.c. power of 35 W/cm^2 on the target, a deposition rates of 9.5 nm/min for Ti and 8 nm/min for Al were achieved for a substrate-source distance of 225 mm. The thicknesses of the Ti and Al layers were determined by a quartz microbalance and were $h_{Ti} \approx 50$ nm and $h_{Al} \approx 10$ nm, respectively. In this paper, the sample is denoted by Si/Ti/Al.

The irradiation was performed in the air with a focused femtosecond laser beam under near-normal incidence to the sample surface. The beam was generated by an ytterbium-doped fibre laser, which operated in TEM$_{00}$ mode, at wavelength $\lambda = 515$ nm and pulse duration $\tau = 300$ fs [23]. In the experiment, the pulse energy values E_p increased gradually from 0.03 µJ to 1.2 µJ. In the case of Gaussian spatial beam profile, from values of pulse energy E_p and beam radius w_0 (at which the beam intensity has fallen to $1/e^2$ of its peak), it is easy to calculate laser fluence as $F = 2E_p/\pi w^2$.

After irradiations, the sample morphology was initially analysed by optical microscopy, and then by scanning electron microscopy (SEM). Elemental composition examination was done by energy-dispersive spectrometer (EDS) connected with the SEM. The surface morphology was additionally scrutinized by a non-contact optical profilometry. The profilometer was equipped with the program that was used for measuring crater depths from two-dimensional (2D) profiles and their three-dimensional (3D) visualization (Zygo corporation, Metro Pro).
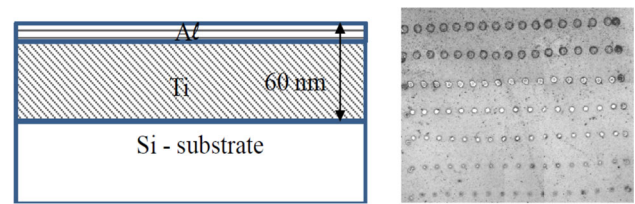

Fig. 1 Schematic views of the BMTF cross section and optical image after the single fs laser pulse irradiation (pulse duration 300 fs, wavelength 515 nm, pulse energy from 0.03 to 0.48 µJ)

3 Results and discussion

The laser irradiation of the sample was done in the way that the 16 single pulses hit the new fresh area of BMTF surface (Fig. 1). The pulse energy was kept constant in each sequence of irradiation. The optical and SEM analyses confirmed almost identical spots on the surface that corresponds to the same pulse energy. In the experiment, we changed the pulse energy discontinuously from 0.03 to 1.2 µJ (E_p [µJ]: 0.03, 0.04, 0.06, 0.08, 0.16, 0.32, 0.48, 0.64, 0.8, 1.0, 1.2). At pulse energies, ranged from 0.03 to 0.32 µJ, circular craters with uniform topography of the irradiated areas were registered. As the pulse energy increased to 1.2 µJ, circular craters were produced too, but with rough topography of the central regions.

After initial examination by both optical microscopy and SEM, profilometry completed qualitative and quantitative analyses of the irradiated areas. Initially, the SEM study provided information about diameters D of the laser spots and their morphologies on the micrometre and nanometre levels. Then, profilometry gave information on their depths, 2D surface profiles and 3D views. Typical morphology of craters registered on BMTF after the single pulse irradiations is presented in the SEM micrographs, Fig. 2. The depth of craters was measured by non-contact optical profilometry (Fig. 3a, b) and elemental composition changes were registered too (Table 1). From all analyses, we found three types of ablations, depending on the values of the single pulse energies E_p:

(i) **_Spallation,_ 0.03 µJ–0.06 µJ.** At the pulse energies $E_p = 0.03$ µJ (Fig. 3a) and $E_p = 0.04$ µJ the uniform layer was removed from the surface of the BMTF and circular shallow craters were formed. At $E_p = 0.06$ µJ the crater centre is slightly different but we can still see similar morphology (Fig. 2). For all three applied pulse energies, the ablation depths (A_d) were around 20 nm (Table 1). This means that the complete first Al layer and a part of the second Ti one were ablated, while the rest of BMTF remained on the Si substrate. This form of craters can be attributed to photomechanical ablation–spallation.

(ii) **_Gentle ablation_, 0.08 µJ–0.32 µJ**. At the pulse energy $E_p = 0.08$ µJ, SEM (Fig. 2) and profilometry revealed a step-like shape of ablated area and this is what we call gentle ablation. The measured step height
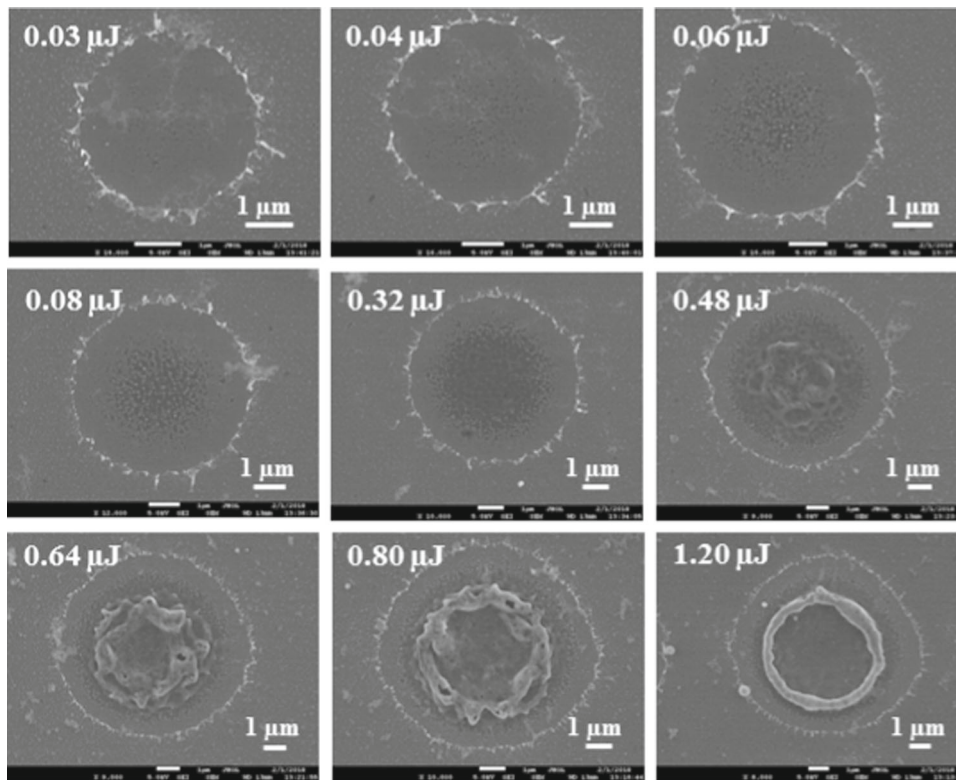
Fig. 2 SEM micrographs of the surface morphology of Si/Ti/Al after single fs pulse irradiations. Energies E_p and the corresponding bars are inserted into each micrograph. The SEM micrographs at $E_p = 0.16$ µJ and 1.0 µJ are similar to 0.32 µJ and 1.2 µJ, respectively, and they are not presented (pulse duration 300 fs, wavelength 515 nm)

and the crater depth were found to be $d = 19.5$ nm and $A_d = 24.3$ nm, respectively (Table 1). Similar morphology can be seen at pulse energy 0.32 µJ (Fig. 3b). The crater depth and step height increase up to $A_d = 46$ nm and $d = 24$ nm (Table 1). In the case of $E_p = 0.16$ µJ similar results were obtained. These results show that for the applied pulse energies BMTF was not completely ablated from the Si substrate.

(iii) **Ablation, 0.48 µJ−1.2 µJ**. At the applied pulse energies, the morphology differs considerably comparing to the previously registered ones. The inner rim can be seen in the bottom three micrographs in Fig. 2. The depths of the centres of the craters were $A_d > 60$ nm (Table 1). These values are greater than BMTF thickness. The problem with the profilometry measurement occurred because of very pronounced inhomogeneous bottoms of the craters at energies $E_p = 0.48$ µJ, $E_p = 0.64$ µJ, and $E_p = 0.80$ µJ. Despite these difficulties, it was possible to measure the values of the crater depths. As the pulse energy further increased, the crater depths increased too. Inhomogeneity of the bottom disappeared at pulse energies $E_p = 1.0$ µJ and $E_p = 1.2$ µJ.

Besides the profilometer analysis, the EDS technique was applied in order to check the quality of registered spallation and ablation of BMTF from Si substrate. Elemental compositions of some of the created craters are shown in Table 1, from which one can see that: (i) nonzero concentration of Al was only present on the non-irradiated BMTF surface, (ii) nearly the same concentrations of Ti were measured in the irradiated areas, at laser pulse energies 0.03 µJ, 0.04 µJ, and 0.06 µJ, (iii) concentration of Ti on the first steps was about the same as in the case of non-irradiated BMTF, (iv) in the central areas of all craters produced by higher pulse energies than 0.48 µJ, the average concentration of Ti was lower, but different from zero.

By means of the three techniques, SEM, profilometry and EDS, we estimated the range of laser pulse energy, at which the upper Al layer and a part of Ti layer were ablated from BMTF. These values belong to the interval 0.03–0.32 µJ.

In this study, the damage threshold for BMTF was estimated. For calculation, only the data concerning spallation and gentle ablation were taken into consideration. This means that in the following calculation we measured the diameters of the first six craters.

The procedure of the ablation threshold calculation is well known for ultra-short Gaussian laser pulses. It uses a linear relationship between the pulse energy and laser fluence F [24,25]. Namely, for a Gaussian spatial beam profile with the beam radius w_0, the maximum laser fluence F_0 in front of the surface depends linearly on the incident laser pulse energy E_p. Maximum laser fluence can be calculated from $F_0 = 2E_p/(\pi w_0^2)$. Diameters (D) of the laser-ablated areas are correlated with F_0 by $D^2 = 2 w_0^2 ln(F_0/F_{Dth})$. As a result,
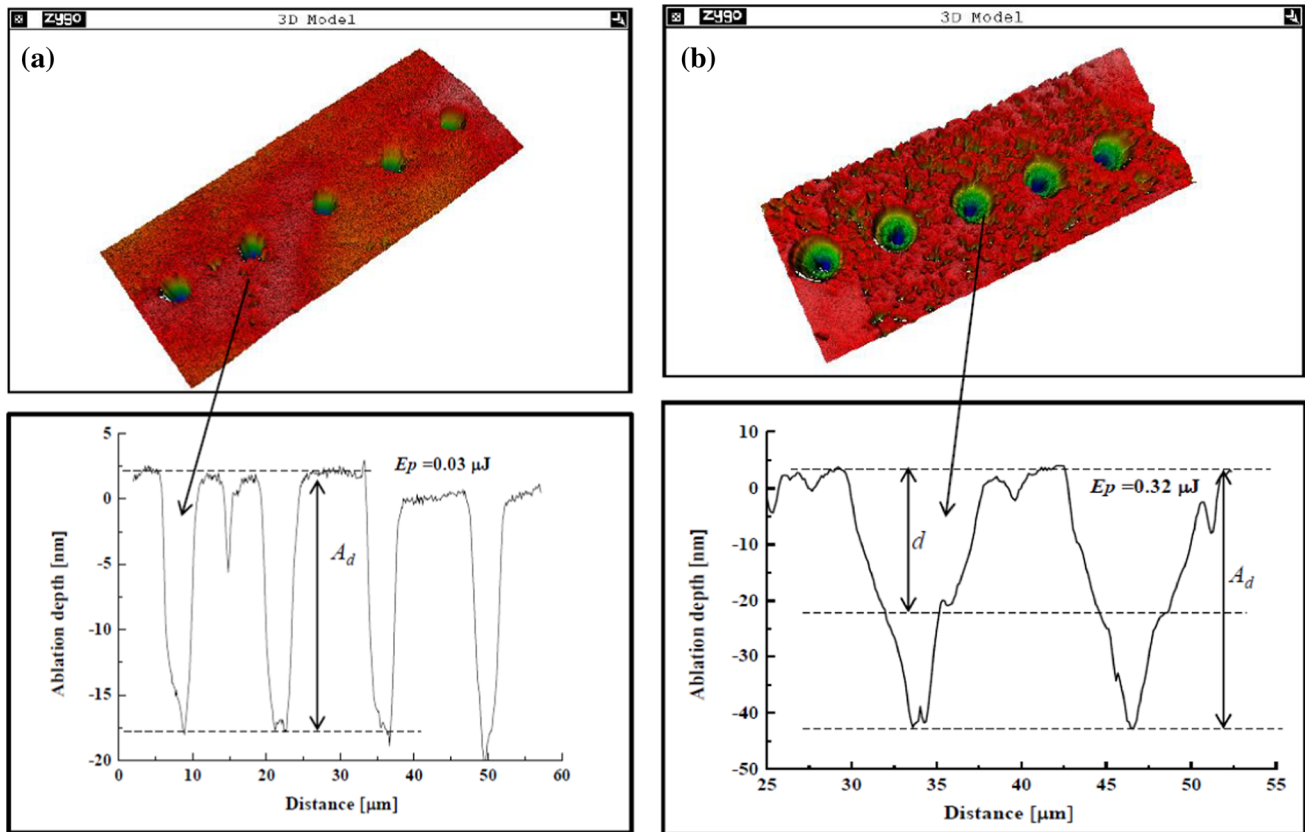
Fig. 3 2D- and 3D-profiles of the craters created by the single laser pulses at (**a**) $E_p = 0.03$ µJ and (**b**) $E_p = 0.32$ µJ. Distances from the bottoms of the ablated areas to the surface A_d are 19 nm and 46 nm, respectively. The distance from the step to the surface d in (**b**) is 24 nm

Table 1 Compositional changes and depths of some craters produced on the Si/Ti/Al after single fs pulse irradiation

E_p(µJ)	F(J/cm^2)	Al (wt%)	Ti (wt%)	Si (wt%)	O (wt%)	A_d(nm)	d (nm)
BMTF		0.24	1.82	95.58	2.37	–	–
0.03	0.20	–	1.86	95.26	2.88	19.0	–
0.04	0.26	–	1.84	95.76	2.40	20.2	–
0.06	0.39	–	1.87	95.86	2.27	21.0	–
0.08	0.53	–	1.76^C	95.42^C	2.82^C	24.3	19.5
			1.84^S	95.82^S	2.76^S		
0.32	2.10		1.41^C	96.05^C	2.55^C	46	24
			1.77^S	95.21^S	3.02^S		
0.48	3.16	–	1.00^C	97.49^C	1.52^C	> 60	
			1.86^S	95.31^S	2.83^S		
1.20	7.9		0.42^C	98.46^C	1.12^C	> 60	
			1.85^S	95.43^S	2.72^S		

from the linearity of D^2 versus applied pulse energies lnE_p, we can determine the Gaussian beam radius w_0 and damage threshold fluence F_{Dth} (Fig. 4). We found $w_0 = 2.78$ µm and damage threshold pulse energy $E_{Dth} = 0.0115$ µJ, which gives $F_{Dth} \approx 0.1$ J/cm^2. This value is in accordance with generally theoretically predicted one [5] for fs laser pulses and a metal surface, specifically, to the spallation threshold for bulk Ti being 0.08J/cm^2 [26].

In our experiment, at $F = 0.2$ J/cm^2, which is greater than F_{Dth}, ablation of BMTF was registered. Because of the form of ablated craters the term "spallation", which describes the dynamic fracture that results when a shock wave strikes a solid sample, is commonly used [16]. The material ejection mainly driven by the relaxation of fs laser-induced stresses is generally referred to as photomechanical spallation [18–22]. It was shown that photomechanical spallation starts at pulse energy/fluence higher than the damage threshold
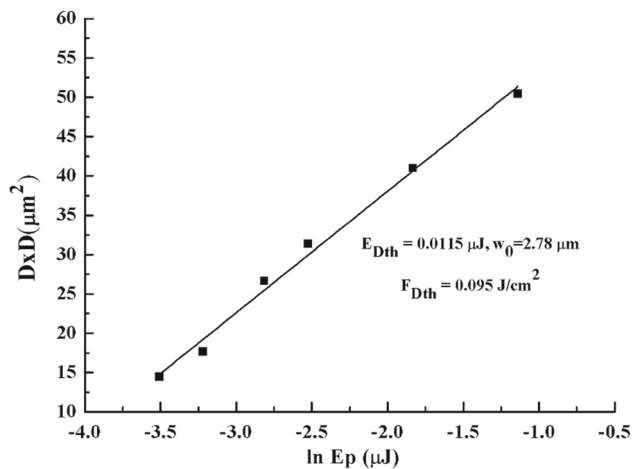
Fig. 4 Squared crater diameter D^2 versus logarithm of laser pulse energy $\ln E_{\mathrm{p}}$. The values of D were averaged over 10 measurements. The Gaussian beam radius w_0 and energy E_{Dth} were determined from the linear least square fit—from the slope and intersection, respectively

value and persists for a particular interval [22]. This interval consists of values for which "gentle" lifting of the surface layer happened. As pulse energy/fluence further increases, severe ablation happens and possible explosive decomposition can be registered. In strongly absorbing materials, such as metals the fast heating and cooling by short laser pulses, as is fs one, can lead to the formation of compressive thermoelastic stress, which can be evaluated using the laser and material parameters. Since two extremely different metals as Al and Ti were combined in BMTF, the buried Ti layer appears as a heat accumulator due to the large electron–phonon coupling factor $g_{\mathrm{Ti}} = 1.3 \times 10^{18}$ $\mathrm{Wm^{-3}K^{-1}}$ [27] and low thermal diffusivity $\chi_{\mathrm{Ti}} = 9 \times 10^{-6}\,\mathrm{m^2/s}$ [28], while the light-absorbing outer Al layer works as a sensitizer, due to its low $g_{\mathrm{Al}} \leq 2.45 \times 10^{17}$ $\mathrm{W\,m^{-3}\,K^{-1}}$ [27] and high $\chi_{\mathrm{Al}} = 9.6 \times 10^{-5}\,\mathrm{m^2/s}$ [28] transferring the absorbed energy to the underlying Ti layer. Under action of an ultra-short pulse with duration $\tau < 1$ ps, as it is in the experiment, the heated layer is formed for the time less than the acoustic relaxation time $t_{\mathrm{ac}} = h_{\mathrm{Ti}}/C_l \approx 10$ ps, where C_l is longitudinal sound speed and $C_l(\mathrm{Ti}) \approx 5$ km/s [28]. Thus, the ultra-short heating $\tau < t_{\mathrm{ac}}$ can be considered as an isochoric process. The heat generated by absorption stays confined in the irradiated volume for the period of the laser pulse and cannot escape via heat conduction. Once the condition for the stress confinement is fulfilled, the stress magnitude can be evaluated as $\sigma \sim \gamma(F/h_{\mathrm{Ti}})$, where γ is the Grüneisen coefficient ($\gamma_{\mathrm{Ti}} \sim 1.2$ and $\gamma_{\mathrm{Al}} \sim 2.5$) [28] with the resulting maximum stress magnitude $\sigma \sim 10$ GPa at $h_{\mathrm{Ti}} = 50$ nm and $F \approx 0.1\,\mathrm{J/cm^2}$. Additionally, in the case of multilayered thin films composed of dissimilar metals, fs laser pulse action causes inhomogeneous heating and cooling. This happens not only because of their different ther-

mophysical properties but also of the presence of the interface between the two metals.

In the experiment, we registered spallation for E_{p}/F values of 0.03, 0.04, 0.06 μJ/0.2, 0.26, 0.39 $\mathrm{J/cm^2}$. The bottoms of these craters are smooth with constant depths. For the next E_{p}/F of 0.08, 0.16, 0.32 μJ/0.59, 1.05, 2.10 $\mathrm{J/cm^2}$ spallation was registered too, but with craters that have a specific shape. The craters consist of flat central parts and step-like edge. The BMTF was not completely ablated, and maximal depth was 46 nm. Further, increase in pulse energy/fluence creates different shapes of the craters. Now, they have bumpy centres and flat steps on their edges. Maximal depths in the centres were higher than BMTF thickness (Table 1). Due to the spatial variation of laser intensity in the Gaussian profile, spallation and phase explosion coexist and together contribute to the material ejection induced by the same laser pulse [21]. This was registered as the pulse energy increased and can be seen at series of SEM micrographs (Fig. 2).

4 Conclusion

In this study, we performed the experiment using the thin nano-layer bimetallic film Si/Ti/Al and laser beam with a pulse duration of 300 fs and wavelength of 515 nm. Irradiation was done in the air atmosphere, with the single laser pulses of different pulse energy/fluence values. Morphological and compositional changes, after single pulse irradiation, were examined with SEM, profilometry, and EDS. In conclusion, single-shot femtosecond laser ablation of the film demonstrates energy-dependent selective removal of the first Al layer and a part of Ti layer without complete removal of BMTF. Depending on the pulse energy/fluence we found that spallation, gentle ablation, and ablation with probable phase explosion took place. Damage/ablation threshold, this parameter is important for the laser processing of BMTF, was calculated to be $F_{\mathrm{Dth}} \approx 0.1\,\mathrm{J/cm^2}$.

Data Availability Statement This manuscript has no associated data or the data will not be deposited. [Authors' comment: All relevant data have been included in the paper.]

References

1. S.M. Petrović, D. Peruško, Laser Modification of Multilayer Thin Films, in *Advances in Optics*: *Reviews Book Series* 4, chapter 7, 169–201. Editor Sergey Y. Yurish, (International Frequency Sensor Association Publishing, 2020)

2. G. Han, S. Zhang, P.P. Boix, L.H. Wong, L. Sun, S.Y. Lien, Prog. Mater Sci. **87**, 246–291 (2017)

3. A.S. Ramos, M.T. Vieira, L.I. Duarte, M.F. Vieira, F. Viana, R. Calinas, Intermetallics **14**, 1157–1162 (2006)

4. V.V. Temnov, Nat. Photonics **6**, 728–736 (2012). https://doi.org/10.1038/NPHOTON.2012.220

5. E.G. Gamaly, A.V. Rode, Prog. Quantum Electron. **37**, 215–323 (2013)

6. J. Bovatsek, A. Tamhankara, R.S. Patel, N.M. Bulgakova, J. Bonse, Thin Solid Films **518**, 2897–2904 (2010). https://doi.org/10.1016/j.tsf.2009.10.135

7. N.T. Goodfriend, S.V. Starinskiy, O.A. Nerushev, N.M. Bulgakova, A.V. Bulgakov, E.E.B. Campbell, Appl. Phys. A **122**, 154–162 (2016). https://doi.org/10.1007/s00339-016-9666-x

8. S.M. Petrović, B. Gaković, D. Peruško, T. Desai, D. Batani, M. Čekada, B. Radak, M. Trtica, Laser Phys. **19**, 1844–1849 (2009). https://doi.org/10.1134/S1054660X09150353

9. J. Jandeleit, G. Urbasch, H.D. Hoffmann, H.-G. Treusch, E.W. Kreutz, Appl. Phys. A **63**, 117–121 (1996)

10. M. Olbrich, E. Punzel, R. Roesch, R. Oettking, B. Muhsin, H. Hoppe, A. Horn, Appl. Phys. A **122**, 215–222 (2016). https://doi.org/10.1007/s00339-016-9736-0

11. S.I. Kudryashov, A.A. Ionin, Int. J. Heat Mass Transf. **99**, 383–390 (2016). https://doi.org/10.1016/j.ijheatmasstransfer.2016.03.097

12. S.I. Kudryashov, B. Gaković, P.A. Danilov, S.M. Petrović, D. Milovanović, A.A. Rudenko, A.A. Ionin, App. Phys. Lett. **112**, 02310 (2018). https://doi.org/10.1063/1.5010793

13. B. Gaković, G.D. Tsibidis, E. Skoulas, S.M. Petrović, B. Vasić, E. Stratakis, J. Appl. Phys. **122**, 223106 (2017). https://doi.org/10.1063/1.5016548

14. K.C. Phillips, H.H. Gandhi, E. Mazur, S.K. Sundaram, Adv. Opt. Photonics. **7**, 684–705 (2015). https://doi.org/10.1364/AOP.7.000684

15. M.V. Shugaev, Chengping Wu, O. Armbruster, A. Naghilou, N. Brouwer, D.S. Ivanov, T.J.-Y. Derrien, N.M. Bulgakova, W. Kautek, B. Rethfeld, L.V. Zhigilei, MRS Bull. **41**, 960–968 (2016)

16. E. Leveugle, D.S. Ivanov, V. Zhigilei, Appl. Phys. A **79**, 1643–1655 (2004). https://doi.org/10.1007/s00339-004-2682-2

17. M.B. Agranat, S.I. Anisimov, S.I. Ashitkov, V.V. Zhakhovskii, N.A. Inogamov, K. Nishihara, Yu.V. Petrov, V.E. Fortov, V.A. Khokhlov, Appl. Surf. Sci. **253**, 6276–6282 (2007)

18. V.V. Shepelev, N.A. Inogamov, S.V. Fortova, Opt. Quantum Electron. **52**, 88–108 (2020). https://doi.org/10.1007/s11082-020-2214-0

19. G. Paltauf, P.E. Dyer, Chem. Rev. **103**, 487–518 (2003)

20. S.I. Ashitkov, N.A. Inogamov, V.V. Zhakhovskii, Yu.N. Emirov, M.B. Agranat, I.I. Oleinik, S.I. Anisimov, V.E. Fortov, JETP Lett. **95**, 176–181 (2012)

21. M.V. Shugaev, L.V. Zhigilei, Comput. Mater. Sci. **166**, 311–317 (2019). https://doi.org/10.1016/j.commatsci.2019.05.017

22. A.A. Ionin, S.I. Kudryashov, A.A. Samokhin, PHYS-USP. **60**, 149–160 (2017)

23. P.A. Danilov, D.A. Zayarny, A.A. Ionin, S.I. Kudryashov, A.A. Rudenko, A.A. Kuchmizhak, O.B. Vitrik, Yu.N. Kulchin, V.V. Zhakhovsky, N.A. Inogamov, JETP Lett. **104**(11), 759–765 (2016). https://doi.org/10.1134/S0021364016230077

24. J. Bonse, P. Rudolph, J. Kruger, S. Baudach, W. Kautek, Appl. Surf. Sci. **154**–**155**, 659–663 (2000)

25. N. Sanner, O. Utéza, B. Bussiere, G. Coustillier, A. Leray, T. Itina, M. Sentis, Appl. Phys. A **94**, 889–897 (2009). https://doi.org/10.1007/s00339-009-5077-6

26. C.S. Nathala, A. Ajami, A.A. Ionin, S.I. Kudryashov, S.V. Makarov, T. Ganz, W. Husinsky, Opt. Express **23**(5), 5915–5929 (2015). https://doi.org/10.1364/OE.23.005915

27. Zh. Lin, L.V. Zhigilei, Phys. Rev. B **77**, 075133 (2008). https://doi.org/10.1103/PhysRevB.77.075133

28. I.S. Grigor'ev, E.Z. Meylikhova (eds.), *Fizicheskie Velichini* (Energoatomizdat, Moscow, 1991)